AIAA Paper No. 72-463

INTERFEROMETRIC DENSITY MEASUREMENTS IN THE ARC OF A PULSED PLASMA THRUSTER

by
K. I. THOMASSEN and D. TONG
Massachusetts Institute of Technology
Cambridge, Massachusetts

AIAA 9th Electric Propulsion Conference

BETHESDA, M D. / APRIL 17-19, 1972

-- NOTES --

INTERFEROMETRIC DENSITY MEASUREMENTS IN THE ARC OF A PULSED PLASMA THRUSTER*

K. I. Thomassen and D. Tong
Massachusetts Institute of Technology
Cambridge, Massachusetts

Abstract

Spatial and temporal measurements of the electron density were made using a He-Ne laser. The multiple pass Mach-Zehnder interferometer detects densities above 10^{15} particles/cm^3. Using these data and free streaming solutions to the Boltzmann equation, which model the expansion of the exhaust, we determine the ion temperature and total charge in the exhaust. The percentage ionization can then be found, and estimates made of the gas dynamic portion of the thrust.

I. Introduction

Pulsed electric thrusters have recently found use in satellite control application[1] and are increasingly being incorporated into design plans for various satellite missions. To increase their use and versatility requires improvements in performance, and hence we initiated a program of diagnostic measurements and design changes on the Teflon fuel thrusters used on the Lincoln Experimental Satellite, LES-6[2,3]. Results of the diagnostic work to date may be found in the literature[4,5].

Earlier measurements determined electron temperature and densities in the exhaust, downstream from the plasma arc which forms over the Teflon surface. To determine the gas dynamic pressure of the plasma on the fuel surface requires a density measurement in the arc. A calculation of this surface pressure was needed to determine the total force on the exhaust. Circuit measurements of the arc current, giving the surface magnetic field, showed that the plasma acceleration could be explained by the magnetic pressure on the arc. Nonetheless, there is sufficient uncertainty that an estimate of the gas dynamic contribution was required to complete the model of this thruster.

In this paper we report an experiment to measure the arc density with a He-Ne laser, and give a theoretical model for the expansion of the exhaust. From the theory and experimental data we determine electron density, total electron charge in the exhaust, and ion temperature. The ions control the plasma expansion so a density measurement with distance determines their temperature. We show that the electron pressure on the plasma contributed to no more than a third of the total force on the exhaust.

II. The Experiment

A multipass Mach-Zehnder interferometer as described by Rizzo[6] is used in this measurement to increase the total path length through the system and improve the sensitivity. The physical arrangement of the mirrors and beam splitters around the vacuum chamber is shown schematically in Fig. 1(a). Multiple-pass mirrors in both the reference and plasma arms equalize the path lengths in these two arms. The beams recombine at an angle θ as shown in Fig. 1(b) to produce fringes which slide past the pinhole collimator as the density is varied. The entire interferometer, including the source and the photodetector, was mounted on a solid aluminum I-beam for rigidity. Optical components with micrometer adjustable mounts were supported by a 3/4" thick aluminum yoke bolted to the I-beam. Micrometer and screw adjustments were found to be indispensable in the alignment of the interferometer.

Since the beam passes through the exhaust plasma at several positions along the arc, we obtain an average of the arc density (in the direction of the current). This presents no problem because we are interested primarily in the density perpendicular to the Teflon face. A diverging lens is used to expand the fringe pattern before it reaches the pinhole, and a polaroid lens attenuates the fringe pattern below the saturation level of the phototube.

The source used is a 3mW, c-w He-Ne laser operating at 6328A. The beam splitters and mirrors are high quality 1/20 λ optical flats, dielectric coated to operate at the laser wavelength. The vacuum windows are flat to 1/10 λ and have anti-reflective coatings to minimize beam attenuation. The phototube, Amperex type XP-1002, has a response linear to within one percent. Both the phototube and the oscilloscope have response times in the nanosecond range.

In spite of the rigid optical specifications, the fringe pattern degrades to an unacceptable level when the beam is reflected for more than 7 passes through the plasma. This degradation is due mainly to the vacuum windows and not to the coherence length of the laser. It was not possible to include the interferometer inside a larger vacuum chamber because the exhaust would contaminate the optical surfaces. Because of this contamination the vacuum windows had to be cleaned periodically.

Vibration of the interferometer was a severe problem when the vacuum chamber was mounted directly on the I-beam. Vibrations from the roughing pump, transmitted through the rubber hose connection to the vacuum chamber and hence to the interferometer, were sufficient to destroy any observable fringe pattern, making alignment virtually impossible. Eventually the interferometer was isolated from the vacuum system, reducing vibration to an acceptable level. The remainder was found to be useful in measuring the amplitude of the fringes. This calibration was needed because the plasma introduced less than 2π radians of phase shift. No errors are introduced in the measurement by the vibration because its period is on the order of milliseconds.

* Experiments were performed at M.I.T. Lincoln Laboratory and sponsored by the Department of the Air Force.

To determine the electron density from the detector signal we combine the electric fields of the two waves shown in Fig. 1(b),

$$E_{1X} = E_1 e^{-j(kz - \phi)}$$
$$E_{2X} = E_2 e^{-j(\alpha z + \beta y)} \quad (1)$$

where $k = 2\pi/\lambda$ is the wavenumber of the laser source and α and β are the z and y components of k. The phase difference ϕ between the two paths includes the plasma contribution which changes by $\Delta\phi$ when plasma is present:

$$\Delta\phi = kd(1 - \sqrt{1 - \omega_p^2/\omega^2})$$
$$\approx \frac{kd}{2} \frac{\omega_p^2}{\omega^2} \quad (2)$$

with ω_p the radian plasma frequency. This phase shift is proportional to density in our experiment. The width d must be replaced by an effective width if the density varies with distance along the beam. This width is found by integrating the density profile and equating it to the peak density times an effective width. The fields in (1), with their associated magnetic fields, give an average Poynting flux whose z-component is

$$\langle P_z \rangle = \frac{1}{2\eta}\left[E_1^2 + E_2^2 + 2E_1E_2(\cos \beta y + \phi)\right] \quad (3)$$

with $\eta = \sqrt{\mu_o/\varepsilon_o} = 377\ \Omega$. The fringes along the y axis and their shift with plasma density can be determined from (2) and (3), since the detected voltage is proportional to (3).

The position of the thruster in the vacuum chamber can be adjusted by an external connecting rod. With the thruster at various positions, oscillographs are taken of the phototube output by triggering the thruster and oscilloscope simultaneously. These oscillographs give the time variation of phase shift at various positions downstream. In Fig. 2 the upper trace shows intensity variations due to vibration while the lower trace shows intensity variations due to the presence of plasma (note the different time scales).

The effective plasma width d_e used at various downstream positions is given in Table I from the theoretical results of the next section. At distances far from the Teflon face the arc looks like a point source so the free streaming solution is a simple gaussian in the coordinates. (See Eq. 7.) Then, d_e increases linearly with time and is given by

$$d_e = \sqrt{\pi}\, v_T\, t$$

where v_T is the ion thermal velocity. At distances on the order of the arc width, d_e is approximated by the arc width of 3 mm, as determined from high speed end-on photos of the plasma luminosity.

Table I Plasma effective width used in the calculation of maximum density

Distance from Teflon Face (mm)	d_e(mm)
1.0	3.0
3.5	3.0
6.0	3.6
8.5	5.1
11.0	6.6
13.5	8.1
16.0	9.6
21.0	11.9
26.0	14.7

By the methods described above we measured the density as a function of time at various distances along the thrust axis. The curves given in Figs. 3 and 4 are averages over data taken from several oscillographs. In each case the beam made 5 passes through the plasma. An average is required because the amplitudes vary from discharge to discharge. The general shape of the curves, however, remains about the same.

Maximum electron density at the Teflon face occurs approximately 0.6 microseconds after initiation of the discharge when the current is a maximum. Assuming $d_e = 3$mm, the peak density is approximately 9.3×10^{16}/cc. Peak densities downstream are less. Figure 5 shows the peak electron density (in time) at any downstream point as a function of distance downstream. The peak density decreases slowly at first, but eventually varies inversely as the cube of the distance. The lowest density (at 20 cm) was measured with the microwave interferometer[3]. Unfortunately densities between 26 mm and 20 cm had to be extrapolated since neither interferometer operates in that range.

All of the oscillographs taken with the beam adjacent to the Teflon face show a reversal of phase shift indicating that the dielectric constant changes from a value less than ε_o to one greater than ε_o. Such a reversal is not seen in any of the oscillographs taken further downstream, so neutral atoms are assumed responsible. If this is the case an estimate of the neutral density near the Teflon face can be made.

The dielectric constant of a gas of neutral particles is given by

$$\varepsilon = \varepsilon_o\left(1 + \frac{N\alpha}{\varepsilon_o}\right)$$

where N is the particle density and α is the polarizability, defined as the ratio of the induced dipole moment of an atom to the applied field. In general, α includes several effects: electronic polarizability due to separation of the electron cloud from the neucleus; ionic polarizability due to separation of atoms in a molecule with ionic bonding; and orientational polarizability due to the tendency of molecules with permanent dipole moment

to orient themselves along the applied field direction. In the ablated teflon gas, we expect mostly single atoms to exist because of the low molecular bonding energy. Hence only the electronic polarizability of carbon and fluorine atoms contributes to the dielectric constant.

A very simple model represents the electrons of an atom by a sphere of uniform negative charge density about the positive neucleus[7]. From this model one finds that α is proportional to the atomic volume. Using this result, the polarizability for the actual gas is predicted to be 3×10^{-41} Farads-m^2, a value between the experimental values for helium and neon.

The magnitude of the reverse phase shift is 0.2 rad., corresponding to $\varepsilon = \varepsilon_o(1 + 2.6 \times 10^{-5})$. Using the assumed value of α, we calculate a neutral density of 7.6×10^{18}/cc.

III. Expansion of the Exhaust

The plasma formed in the discharge arc expands, free from collisions, into the vacuum surrounding the thruster. This expansion is governed by the expansion of the ions, hence a free streaming solution of the Boltzmann equation for the ion distribution determines the parameters describing the exhaust. In particular, comparing our measurements with the results of the theory gives both the average ion exhaust velocity and ion temperature.

Before giving the free streaming solutions we show that a collision model gives answers which are in contradiction with the interferometer data. The force free Boltzmann equation with a simple collision model is

$$\frac{\partial f}{\partial t} + \bar{v} \cdot \nabla f = -\nu(f - f_o) \tag{4}$$

From the first two moments of this equation one obtains the usual equations of continuity of mass and motion, which combine to give

$$\frac{\partial n}{\partial t} + D\nabla^2 n = 0 \tag{5}$$

where n is the ion density, $D = v_T^2\tau$ is a diffusion coefficient describing the collision process (relaxation time τ). Solutions to (5) assuming an initial point source of particles is

$$n \propto t^{-3/2} \exp\left[-\frac{x^2 + y^2 + z^2}{4v_T^2\, t\, \tau}\right] \tag{6}$$

The free streaming solutions to (4) (with $\nu = 0$) are

$$n \propto t^{-3} \exp\left[-\frac{x^2 + y^2 + z^2}{v_T^2\, t^2}\right] \tag{7}$$

For times $t > 4\tau$ the free streaming solution dominates. During arc formation of course, collisions dominate and establish a quasi-equilibrium. Consequently, to describe the exhaust we must use the free streaming solutions. In addition, since the plasma is created at the surface during a finite time period we must convolve the impulse solution just given with the source function, determined by measurement. These solutions can then be fitted to density measurements downstream to determine the parameters of interest, which we now proceed to do.

For a given group of particles, the equilibrium distribution to which they relax via collisions is the Maxwellian. Further, while the arc is forming the particles are accelerating, but when the arc formation is complete we assume the particles have acquired a constant drift velocity superimposed on the Maxwellian distribution. The distribution function is then of the form

$$f \propto \exp\left[-\frac{1}{v_T^2}\left[(v_x - v_o)^2 + v_y^2 + v_z^2\right]\right] \tag{8}$$

where the ion thermal velocity is v_T, and v_o is the drift velocity along the thrust axis (x axis).

We are interested in the region $x > 0$ where, initially, f is identically zero. Plasma is being generated in the arc which is placed at $x < 0$. The boundary $x = 0$ can be chosen arbitrarily as some point where density data $n_o(t)$ is available. With the assumption made above on the velocity distribution, the boundary condition on f is

$$f_o = f\Big|_{x=0} = An_o(t)g(y)h(z)\exp\left[-\frac{1}{v_T^2}\left[(v_x - v_o)^2 + v_y^2 + v_z^2\right]\right] \tag{9}$$

where $g(y)$ and $h(z)$ are as yet unspecified functions and A is a normalizing constant. This expression holds only for $v_x > 0$ and is identically zero for $v_x < 0$. Physically, all particles enter the region $x > 0$ through the $x = 0$ plane with positive velocities. This restriction becomes important when f is later integrated over velocity to obtain the particle density n.

Solutions to Eq. 4 in the absence of collisions are obtained by the method of characteristics. For all $x > 0$, f is given by

$$f = f_o\left[y - \frac{v_y x}{v_x},\ z - \frac{v_z x}{v_x},\ \bar{v},\ t - \frac{x}{v_x}\right] \tag{10}$$

as can be verified by direct substitution. It follows then that the solution we seek is

$$f(\bar{r},\bar{v},t) = An_o\left(t - \frac{x}{v_x}\right)\, g\left(y - \frac{v_y x}{v_x}\right)\, h\left(z - \frac{v_z x}{v_x}\right) \cdot \left(\frac{1}{\sqrt{\pi}\, v_T}\right)^3 \exp\left[-\frac{1}{v_T^2}\left[(v_x - v_o)^2 + v_y^2 + v_z^2\right]\right] \tag{11}$$

which satisfies the boundary condition at $x = 0$.

Theoretically, we could integrate f over velocity to obtain the density as a function of space and time, but since the exact forms of g and h are unknown integration is impossible. A different approach is taken here whereby the half space $x > 0$ is divided into three sections; the near, mid, and far regions. In the near region, adjacent to the discharge arc, the source is planar. In the mid region the arc appears to be a line source, while the far region is where the arc is a point source. Boundary conditions in these regions are:

$$f_o = \begin{cases} n_o A_1 \exp[\bar{v}] & \text{(near region)} \\ n_o A_2 \exp[\bar{v}]\ \delta(z) & \text{(mid region)} \\ n_o A_3 \exp[\bar{v}]\ \delta(y)\ \delta(z) & \text{(far region)} \end{cases}$$

where

$$\exp[\bar{v}] = \exp\left[-\frac{1}{v_T^2}\left[(v_x - v_o)^2 + v_y^2 + v_z^2\right]\right]$$

In each region f is still given by Eq. 10.

Since $n_o(t)$ is an experimentally determined function, $n(\bar{r},t)$ can be obtained only by numerical integration of f. Alternatively, it is equally valid first to obtain the solution to a time impulsive source, and then to convolve it with $n_o(t)$ to obtain $n(\bar{r},t)$. One can obtain considerable information from the impulse response without carrying out the convolution. Therefore, Table II lists the distribution function f_i and density n_i for a time impulse source in each of the three regions. In each region, the actual density $n(\bar{r},t)$ is given by

$$n(\bar{r},t) = \int_o^t n_o(\tau)\ n_i(\bar{r},t-\tau)\ d\tau \qquad (12)$$

where n_i is the time impulsive solution for that particular region.

For the parameters of this plasma, the duration of the time impulsive response for the first 25 mm in the exhaust is short compared to the duration of the source (see Fig. 6). Consequently, the convolution will give a maximum density when the impulse response occurs at the time when the source function is a maximum. This maximum is simply the area under the curve of the impulse response at the distance in question, times the peak source density. To evaluate the integrals of $n_i(t)$ in Table II is difficult, hence we obtain a lower bound on this area by computing the peak value in time of the impulse response. This technique predicts x^{-1}, x^{-2}, and x^{-3} dependences of the peak density through the three regions. For the far region this technique is exact because the actual density approaches the impulse solution.

The mid and far region solutions in Table II both have the same gaussian dependence in the transverse dimension. The interferometer measurements give no information on the transverse variation of density, but from previous Faraday cup current measurements this data is available. The maximum of the collected current (in time) as a function of distance across the beam is a gaussian with a 1/e width of 8.4 cm at a distance of 15.2 cm from the arc. To test our theoretical results we will derive an expression for that maximum current.

The ion current in the x direction, J_x, is related to the distribution function f by the equation

$$J_x = e\iiint v_x f\ d\bar{v}$$

Carrying out the integral using the far region distribution function yields

$$J_x = eA\frac{x^2}{t^5}\exp\left[-\frac{1}{v_T^2 t^2}\left[(x - v_o t)^2 + y^2 + z^2\right]\right]$$

The time when the maximum current occurs at a fixed position x is given by

$$t_{mJ} = \frac{x\eta}{v_o}$$

where, for $M = v_o/v_T$,

$$\eta = M\zeta = \frac{M^2}{5}\left[\sqrt{1 + \frac{10}{M^2}\left(1 + \frac{z^2}{x^2}\right)} - 1\right] \qquad (13)$$

Far from the source but near the thrust axis ($z \ll x$) the peak collected ion current perpendicular to the arc and to the exhaust, $J_{mx}(x,y = 0,z)$, is given by

$$J_{mx}(x,y = 0,z) \propto x^{-3}\exp\left[-(z/\zeta\, x)^2\right] \qquad (14)$$

This gaussian dependence with z and the x^{-3} dependence at $z = 0$ was verified by the Faraday cup current measurement.

An estimate of total charge in the exhaust can be made by integrating the ion flux $n(x,t)v_x$ crossing an arbitrary x-plane to infinite time. Having measured $n(t)$ at some point x, we can express the particle distribution function at that plane using Eq. 9,

$$f_o = AT(t)\ g(y)\ h(z)\ \exp[\bar{v}]$$

where T is proportional to the measured density variation and we normalize T, g, and h to have a peak value of unity. The constant A is related to the maximum measured density n_{mt}. Since

$$n_{mt} = \int_o^\infty dv_x \int_{-\infty}^{\infty} dv_y \int_{-\infty}^{\infty} dv_z\ f_o \Big|_{T,g,h\,=\,1}$$

we have

$$A = \frac{n_{mt}}{\int_0^\infty dv_x \int_{-\infty}^\infty dv_y \int_{-\infty}^\infty dv_z \exp[\bar{v}]} \qquad (15)$$

The total current crossing the x-plane is given by

$$J_x = eAT(t)\, g(y)\, h(z) \int_0^\infty dv_x \int_{-\infty}^\infty dv_y \int_{-\infty}^\infty dv_z\, v_x \exp[\bar{v}] \qquad (16)$$

Integrating J_x over t, y and z, we get the total charge Q passing the x-plane.

$$Q = \int_{-\infty}^\infty dt \int_{-\infty}^\infty dy \int_{-\infty}^\infty dz\, J_x \qquad (17)$$

Combining Eqs. 15, 16, and 17 and carrying out the integration over $\bar{v}$,

$$Q = en_{mt}v_o \left[1 + \frac{1}{2M} \frac{e^{-M^2}}{\frac{\sqrt{\pi}}{2} + \psi(M)}\right] \int_{-\infty}^\infty dt \int_{-\infty}^\infty dy \int_{-\infty}^\infty dz\, \mathrm{Tgh}$$

where $M = v_o/v_T$ and $\psi(M) = \int_0^M \exp(-s^2)ds$.

IV. Comparison of Theory and Data

In this section we compare our calculations with the data to determine the applicability of the model and to give values for some of the exhaust parameters. The predicted variation of maximum density with distance is verified and the extent of the three solution regions is found. Values of v_T, v_o, and Q are then calculated. Finally, with the estimated values of v_o and v_T, the convolution integral given by Eq. 12 is carried out numerically.

The experimentally determined variation of maximum density (in time) in the thrust direction is shown in Fig. 5, where the curve decreases slowly at first but ultimately varies as the inverse cube of the distance. From the plot, using the expected x^{-1}, x^{-2}, and x^{-3} dependences, we deduce that the near region extends from 1 - 5 mm, the mid region from 10 - 20 mm, and the far region from 25 mm on. By comparison, the arc dimensions are about 25 mm in length (y direction) and 3 mm in width (z direction).

An estimate of $M = v_o/v_T$ can be made by examining the variation of peak ion current across the exhaust. Comparing the Faraday cup data with Eq. 14 gives $\zeta = 0.28$. Using Eq. 13 with $z \ll x$, we find $M \approx 3$.

This estimate of M assumes a single drift velocity for the exhaust. However, there are multiply ionized particles in the plasma with different drift velocities. The more highly ionized particles drift at higher velocities, and since ion current is proportional to both the particle charge and velocity, the Faraday cup data is weighed in favor of the multiply ionized particles. This weighing is evidenced by the fact that the arrival time of peak current corresponds to a speed of 40 km/sec, whereas the average speed of all the ionized particles is approximately 30 km/sec. Hence the actual value of M is probably lower by an amount dependent on the percentage of multiply ionized particles.

Having the above value of M, we can derive v_o and v_T from the expression in Table II for t_m, the arrival time of peak density. Note that in the far region, for $M^2 \gg 1$, $t_m \approx x/v_o$. The maximum density at 20 cm, as measured by the microwave interferometer, occurs at 6.5 microseconds. The peak arc density occurs at 0.5 microseconds. Hence an elapsed time of 6.0 microseconds is chosen for t_m. Using the far region expression for t_m with $M = 3$, we find

$$v_T = 9.3 \text{ km/sec}$$
$$v_o = 27.9 \text{ km/sec} \qquad (18)$$

This value for v_o is in good agreement with experimental evidence so far. The thermal velocity corresponds to an ion temperature of 7.6 eV for ions having a mass of 16.7 atomic units, an average for 2 carbon and 4 fluorine atoms. The estimate for v_T is low since the estimate of M is expected to be high.

With these values of v_o and v_T, the convolution given by Eq. 12 can be carried out numerically to obtain predicted density as a function of time for comparison with data. Since we want to avoid the region where the arc is formed, we take the left boundary plane of the solution region to be the plane at 6 mm away from the Teflon face. The solution downstream is arrived at by numerically convolving the density data at the boundary with the appropriate time-impulsive solution as given in Table II. The normalizing constant A_i (i = 1, 2, or 3 corresponding to near, mid, or far region) is found by integrating f_o over velocity and matching the result to n_o. In the cases of the mid and far regions, it is necessary to multiply the constant by the effective plasma cross section because of the spatial impulse approximation. Hence,

$$A_1 = v_T^{-3}\, \pi^{3/2} \qquad \text{(near region)}$$
$$A_2 = d_e A_1 \qquad \text{(mid region)}$$
$$A_3 = d_e d_g A_1 \qquad \text{(far region)}$$

where d_e is the effective plasma width in the z direction and d_g is the effective plasma width in the y direction (parallel to arc). Only the near and mid region solutions apply in the following calculations since data is not available more than 25 mm from the Teflon face. Figure 6 shows the

measured density at 6 mm and the impulse responses at various distances downstream. Calculated and measured density curves are shown in Fig. 7. The convolved curve at 8.5 mm (Fig. 7a) uses the near region solution while the convolved curves at 13.5 mm (Fig. 7b) and at 16 mm (Fig. 7c) use the mid region solution. In each case the curves are similar in shape but the theoretical curves peak higher than the measured ones. This discrepancy may reflect too low an estimate of v_T, the neglect of recombination, or that the source was approximated by an impulse in space. Carrying out the convolution with v_T arbitrarily increased by 50% did not result in significant change in this difference. The possibility of significant recombination is inferred from Figs. 7 where the ratio of measured peak density to calculated peak density decreases with distance from the Teflon face.

The total charge Q is given theoretically by Eq. 18. Since we need to know only the areas under the curves T, g, and h to compute Q, we can approximate them by square pulses of unit magnitude and some estimated effective widths. The effective width of the pulse approximating h(z), for example, is the value of d_e given earlier. Since $M \approx 3$, the quantity in brackets in Eq. 18 is approximately 1. Hence Eq. 18 reduces to

$$Q \approx en_{mt}v_o d_T d_g d_e \qquad (19)$$

where the d's represent the effective widths. Estimated values of Q and the associated effective widths are listed in Table III. For comparison, the total charge derived by integrating over the Faraday cup current is also given. The steady decrease in estimated values of Q gives further evidence that significant recombination occurs.

V. Summary

An extensive study has been done at M.I.T. Lincoln Laboratories on the solid Teflon plasma thruster, including the development of a circuit model and its analysis, and several plasma diagnostic experiments. However, density measurements, using Langmuir probes and a microwave interferometer, failed to reveal the particle density in the discharge arc, without which it is impossible to estimate the relative importance of gas dynamic and magnetic forces. So, the laser interferometer described in this paper was constructed and used to make the desired electron density measurements. The peak electron density in the arc was found to be 9.3×10^{16}/cc.

The gas dynamic pressure can be calculated assuming the ion density is approximately equal to the measured electron density. We determined that the ion temperature is 7.6 eV, and measurements of the electron temperature give rough values of 15 eV, hence the peak electron and ion gas dynamic pressure is approximately $4.5 \times 10^5 N/m^2$. This pressure is higher than the estimated magnetic pressure[1], $1.6 \times 10^5 N/m^2$. But, since it acts over a smaller area, namely the plasma effective width, the total force it exerts on the Teflon is the same as the total magnetic force. Recent data[7] confirms this equal division when operating at the 5.5 μlb sec impulse level.

The laser interferometer yields data up to 2.5 cm from the Teflon face. The phase data obtained actually gives the electron density integrated along the transverse (z) axis. Density information is derived by assuming that the transverse variation is Gaussian with some estimated effective width. Figures 3 and 4 give the density as a function of time and of distance along the thrust (x) axis. A two dimensional presentation of this data can be given by plotting constant density contours on the x-z plane. These curves, obtained with the aid of a computer, are shown in Fig. 8.

In the far region, the time impulsive solutions apply directly if the source duration is short compared to the travel time. Figures 9 and 10 show contour curves of constant density using this solution. In Fig. 9 these curves are connected smoothly onto the measured density contours given in Fig. 8. Since the far region distribution function is an expanding, drifting Maxwellian, the contours are expanding circles in a coordinate system moving with the drift velocity (Fig. 10).

Several experimental results agree with predictions from this model. The theoretical solutions predict that peak density should decrease with distance by less than x^{-1} in the near region, by less than x^{-2} in the mid region, and as x^{-3} in the far region. Ion current is predicted to have a gaussian dependence in the transverse (z) direction and an inverse cube dependence in the thrust (x) direction. Both of these dependences are verified by Faraday cup data. Finally, our model shows that it is possible, by applying convolution, to project downstream densities using upstream data. In Fig. 7 the density curves obtained in this manner agree in shape with measured density curves and they differ in peak magnitude by a factor less than 2.

Comparing the Faraday cup data with the derived expression for ion current in the far region, we estimate a mach number M = 3, using the ratio of ion drift and thermal velocities. However, since the plasma contains multiply ionized particles traveling at higher than average velocities, we expect this estimate to be somewhat high.

The far region impulsive solution gives an expression for t_m, the time of peak density occurrence (see Table II). For M = 3, and using the value of t_m derived from the microwave interferometer data, we obtain v_o = 27.9 km/sec, and hence v_T = 9.3 km/sec. These values agree with previous experimental data.

A formula is derived relating the total charge passing some plane to the density at that plane. Applying this formula we obtain estimates of total charge on the order of that derived from the integration of Faraday cup current. Two observations suggest that significant recombination takes place in the exhaust. First, the estimates of total charge given in Table III show a steady decrease with distance; and second, in Fig. 7, the ratio of peak measured density to peak calculated density decreases with distance.

Questions that still need to be investigated further include how the neutral density varies with time, and what percentage of multiply ionized particles are in the exhaust. These data are needed to improve the estimates made in this paper.

Table II Theoretical Solutions to Time Impulsive Sources

	Near Region	Mid Region	Far Region
f_o	$A_1\,\delta(t)\,\exp[\bar{v}]$*	$A_2\,\delta(t)\,\delta(z)\,\exp[\bar{v}]$	$A_3\,\delta(t)\,\delta(y)\,\delta(z)\,\exp[\bar{v}]$
f_i	$f_o\left(t-\frac{x}{v_x}\ ,\ v\right)$	$f_o\left(t-\frac{x}{v_x}\ ,\ z-\frac{v_z x}{v_x}\ ,\ \bar{v}\right)$	$f_o\left(t-\frac{x}{v_x}\ ,\ y-\frac{v_y x}{v_x}\ ,\ z-\frac{v_z x}{v_x},\ \bar{v}\right)$
n_i	$A_1\,v_T^{\,2}\,\pi\,\frac{x}{t^2}\exp\left[-\left(\frac{x-v_o t}{v_T t}\right)^2\right]$	$A_2\,v_T\,\sqrt{\pi}\,\frac{x}{t^3}\exp\left[\frac{-1}{v_T^{\,2}t^2}\left[(x-v_o t)^2+z^2\right]\right]$	$A_3\,\frac{x}{t^4}\exp\left[\frac{-1}{v_T^{\,2}t^2}\left[(x-v_o t)^2+y^2+z^2\right]\right]$
t_m**	$\frac{x}{v_o}\left[\frac{M^2}{2}\left(\sqrt{1+\frac{4}{M^2}}-1\right)\right]$***	$\frac{x}{v_o}\left[\frac{M^2}{3}\left(\sqrt{1+\frac{6}{M^2}}-1\right)\right]$	$\frac{x}{v_o}\left[\frac{M^2}{4}\left(\sqrt{1+\frac{8}{M^2}}-1\right)\right]$

* $\exp[\bar{v}] = \exp\left[\frac{-1}{v_T^{\,2}}\left[(v_x-v_o)^2+v_y^{\,2}+v_z^{\,2}\right]\right]$

** Time of occurrence of maximum density ($y = 0,\ z = 0$) found by differentiating $n(\bar{r},t)$ with respect to t.

*** $M = v_o/v_T$

Table III Estimate of Total Charge Released

Distance from Teflon Face	t_T*(μsec)	d_g(cm)	d_e(cm)	n_{mt}(x10^{16}/cc)	Q(x10^{-3} Coul)
3.5 mm	1	2.5	.30	6.0	21.6
6.0 mm	1	2.5	.36	3.1	13.4
11.0 mm	1	2.8	.66	1.4	12.4
16.0 mm	1	3.0	.96	.7	9.7
15.2 cm**					5.3

* As estimated from Fig. 11.

** From Faraday Cup Measurements[5]

References

1. R. J. Vondra, K. I. Thomassen, and A. Solbes, "A Pulsed Electric Thruster for Satellite Control," IEEE 59, pg. 271 (1971).

2. W. J. Guman and P. E. Peko, "Solid Propellant Pulsed Plasma Microthruster Studies," J. Spacecraft and Rockets, 5, pg. 732 (1968).

3. W. J. Guman and D. M. Nathanson, "Pulsed Plasma Microthruster System for Synchronous Orbit Satellites," J. Spacecraft and Rockets, 7, pg. 409 (1970).

4. R. J. Vondra, K. I. Thomassen, and A. Solbes, "Analysis of a Solid Teflon Pulsed Plasma Microthruster," J. Spacecraft and Rockets, 7, pg. 1402 (1970).

5. K. I. Thomassen and R. J. Vondra, "Exhaust Velocity Studies of a Solid Teflon Pulsed Plasma Thruster," J. Spacecraft and Rockets, 9, pg. 861 (1972).

6. J. E. Rizzo, "Electron Density of Relativistic Electron-Beam Produced Plasmas," J. Applied Physics, 41, pg. 4941 (1970).

7. R. J. Vondra and K. I. Thomassen, "Performance Improvements in Solid Fuel Microthrusters," AIAA 10th Aerospace Sciences Meeting, (January 1972), AIAA Paper No. 72-210.

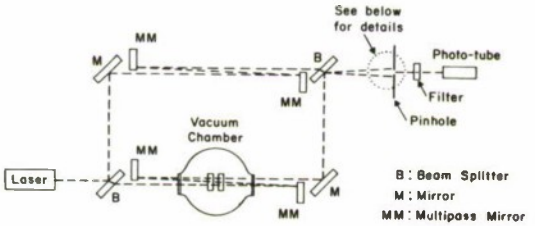

Fig. 1(a) Schematic of M-Z interferometer with source and photodetector.

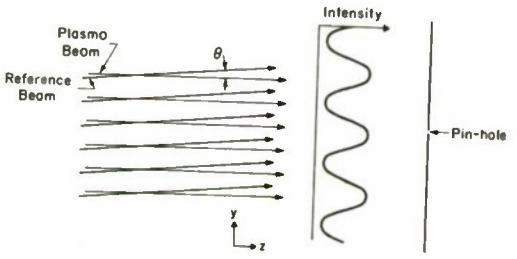

Fig. 1(b) Expanded view of the recombined beam showing size of pinhole in relation to period of intensity variation.

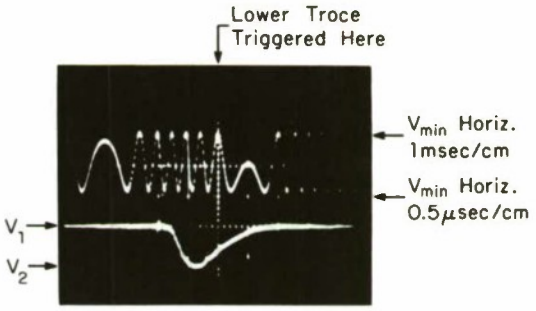

Fig. 2 Typical oscilloscope traces. Upper trace indicates phase changes due to mechanical vibrations. Lower trace indicates phase changes due to the presence of plasma.

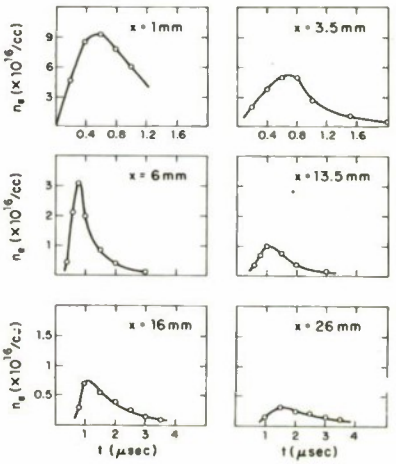

Fig. 3 Curves of measured density as a function of time at various downstream positions.

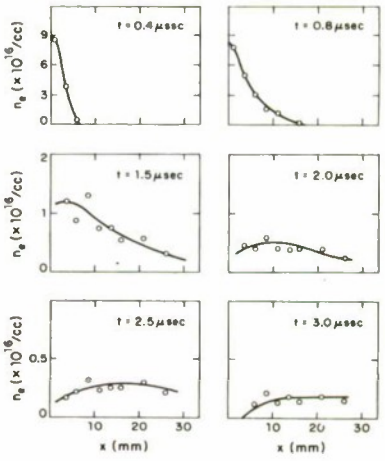

Fig. 4 Curves of measured density as a function of distance along thrust axis at various times.

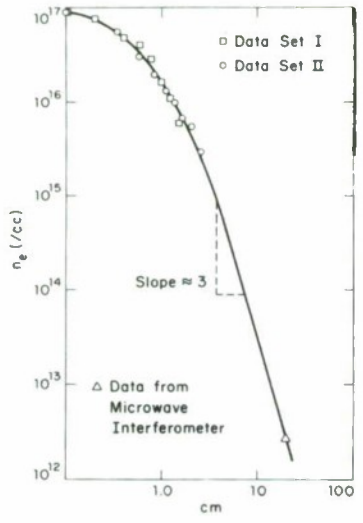

Fig. 5 Variation of maximum measured density as a function of downstream position.

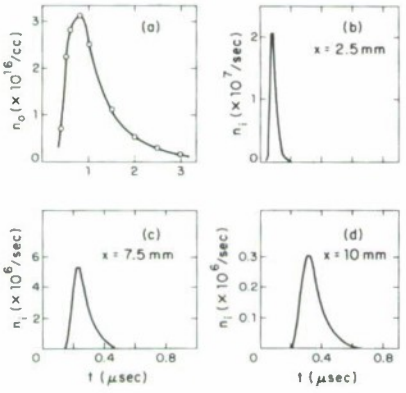

Fig. 6 (a) Measured density at 6 mm from Teflon face; $n_o(t)$
(b) Near region impulse response; $n_i(t)$
(c), (d) Mid region impulse response; $n_i(t)$

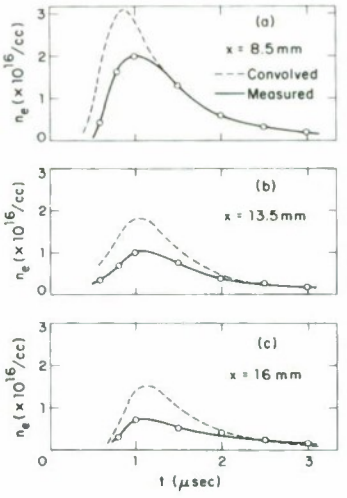

Fig. 7 Comparison of convolved and measured density curves.

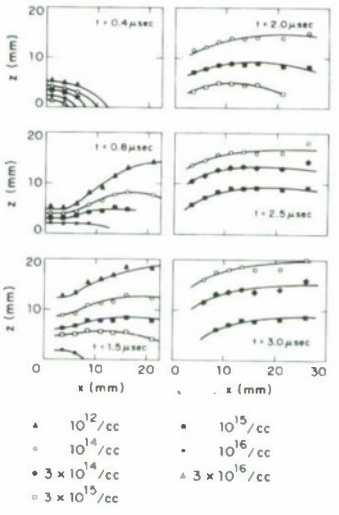

Fig. 8 Computer plotted constant density contours using collected data.

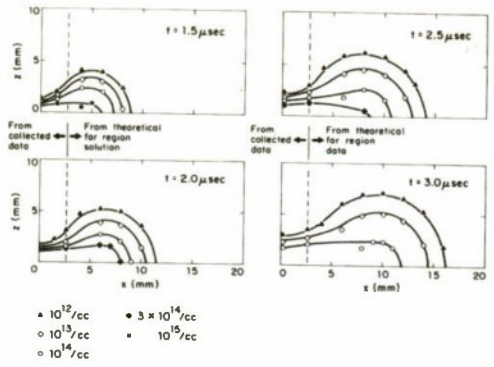

Fig. 9 Constant density contours connecting data to theoretical solution.

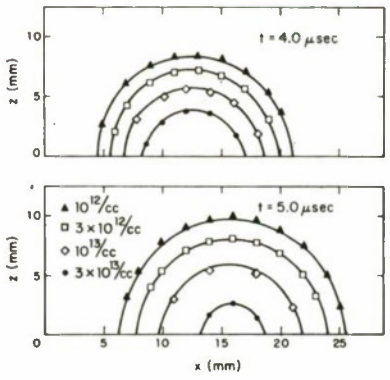

Fig. 10 Constant density contours using far region impulse solution.

UNCLASSIFIED
Security Classification

DOCUMENT CONTROL DATA – R&D

(Security classification of title, body of abstract and indexing annotation must be entered when the overall report is classified)

1. ORIGINATING ACTIVITY (Corporate author)	2a. REPORT SECURITY CLASSIFICATION
Lincoln Laboratory, M.I.T.	Unclassified
	2b. GROUP: None

3. REPORT TITLE

Interferometric Density Measurements in the Arc of a Pulsed Plasma Thruster

4. DESCRIPTIVE NOTES (Type of report and inclusive dates)

Meeting Speech Reprint

5. AUTHOR(S) (Last name, first name, initial)

Thomassen, Keith I. Tong, David

6. REPORT DATE	7a. TOTAL NO. OF PAGES	7b. NO. OF REFS
17 April 1972	10	7

8a. CONTRACT OR GRANT NO.	9a. ORIGINATOR'S REPORT NUMBER(S)
F19628-70-C-0230	MS-3282
b. PROJECT NO.	9b. OTHER REPORT NO(S) (Any other numbers that may be assigned this report)
c.	
d.	ESD-TR-72-112

10. AVAILABILITY/LIMITATION NOTICES

Approved for public release; distribution unlimited

11. SUPPLEMENTARY NOTES	12. SPONSORING MILITARY ACTIVITY
AIAA Paper No. 72-463	Air Force Systems Command, USAF

13. ABSTRACT

Spatial and temporal measurements of the electron density were made using a He-Ne laser. The multiple pass Mach-Zehnder interferometer detects densities above 10^{15} particles/cm^3. Using these data and free streaming solutions to the Boltzmann equation, which model the expansion of the exhaust, we determine the ion temperature and total charge in the exhaust. The percentage ionization can then be found, and estimates made of the gas dynamic portion of the thrust.

14. KEY WORDS

Pulsed plasma thruster Interferometric density Arc density

UNCLASSIFIED
Security Classification